Acta metall. mater. Vol. 41, No. 10, pp. 3017–3027, 1993
Printed in Great Britain.

0956-7151/93 $6.00 + 0.00

DETERMINATION OF THE INTERFACIAL TENSION BY ZERO CREEP EXPERIMENTS ON MULTILAYERS—II. EXPERIMENT

D. JOSELL† and F. SPAEPEN

Division of Applied Sciences, Harvard University, Cambridge, MA 02138, U.S.A.

(Received 18 December 1992)

Abstract—Tensile creep tests were conducted between 700 and 800°C on free-standing silver–nickel multilayered thin films with individual layer thicknesses between 0.5 and 1.3 μm. At different loads, both negative and positive strain rates were measured, from which the zero creep load was determined by interpolation. The zero creep load was found to be proportional to the number of bilayers in the film. The interfacial tension was obtained from the zero creep load per bilayer using a newly developed kinetic model for Coble creep in a multilayer [D. Josell and F. Spaepen, *Acta metall. mater.* **41**, 3007 (1993)]. The correction factors in the model involve the aspect ratio of the grains (determined directly by electron microscopy) and the ratios of the interfacial tension to the grain boundary tensions (determined from the groove angles in the electron micrographs). The tension of the silver–nickel (111) epitaxial interface was found to be 0.76 ± 0.12 J/m^2.

1. INTRODUCTION

In the preceding paper a method for the direct measurement of the interfacial free energy, or interfacial tension, by zero creep experiments on multilayered thin films is described. In this paper, the results of an experimental test of the method by tensile creep on silver–nickel multilayers are presented.

This system was chosen for several reasons. (i) The mutual solubility of the two elements in their crystalline state is extremely low. This enhances the stability of the layers by lowering the coarsening rate, and eliminates potential artifacts in the creep measurements due to changes in solute concentrations. (ii) There are no intermetallic compounds. Their formation would disrupt the interfaces and produce artifacts in the creep measurements. (iii) There is a temperature range in which the creep rates of silver and nickel are both measurable. For the conditions (stress, temperature, microstructure) used in the present work, Coble creep is the dominant mechanism [1]. (iv) Silver and nickel have the same crystal structure (f.c.c.), and can be deposited epitaxially with a strong (111) texture. The measured tension is therefore that of a particular, well-defined interface. (v) Calculations have been made of the tension for this same type of interface [2, 3].

2. EXPERIMENTAL

Multilayers of silver and nickel were deposited in a dual gun electron beam evaporator using charges of 99.99% pure silver and 99.99% pure nickel. The base pressure before a typical run was less than 2×10^{-7} torr. During deposition, pressures were usually less than 3×10^{-6} torr. The multilayers were deposited using shutters to expose the substrates alternately to the evaporating silver and nickel charges. They were removed from their substrates by dissolving a pre-deposited aluminum backing layer in sodium hydroxide. Further details of the preparation process can be found in Ref. [6]. Most of the films consisted of nickel outer surfaces and N bilayers of silver and nickel. Some experiments were done with silver outer layers. N was varied between 0 and 21.

With the exception of the silver layers closest to the surface, all layers of nickel and silver in the same specimen were equally thick. Since at elevated temperatures some depletion of the outermost silver layers due to evaporation was observed, the outermost silver layers, adjacent to the surface nickel layers, were made twice as thick as the other layers (see Fig. 1). The bilayer thickness was varied between 1.0 and 2.6 μm in different multilayers. Figure 1 shows cross-sections of an as-deposited sample. The test specimens were made into a dogbone shape by deposition through a mask. They had a width of 2.0 cm in the grips and a rapid reduction in width to the 1.0 cm wide active region. All corners were rounded to reduce stress concentrations that might lead to ripping of the films. The active area of all films was 2.5 cm long and 1.0 cm wide. Rectangular specimens wrinkled along the tensile direction during the creep tests because of the lateral constraints imposed by the grips. In dogbone specimens, the wrinkles remained restricted to the grip region and the active section was wrinkle-free. The total film thickness varied between 5 and 25 μm depending on both the number of bilayers and the bilayer thickness. The

†Present address: NIST, Gaithersburg, MD 20899, U.S.A.

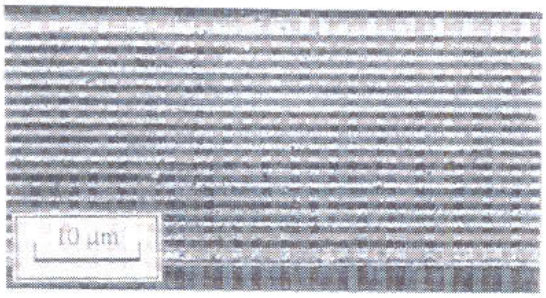

Fig. 1. SEM image of a portion of the cross-section of an as-deposited silver–nickel multilayer consisting of 18 bilayers of silver (bright) and nickel (dark) with nickel caps. The sacrificial subsurface silver layers are of double thickness.

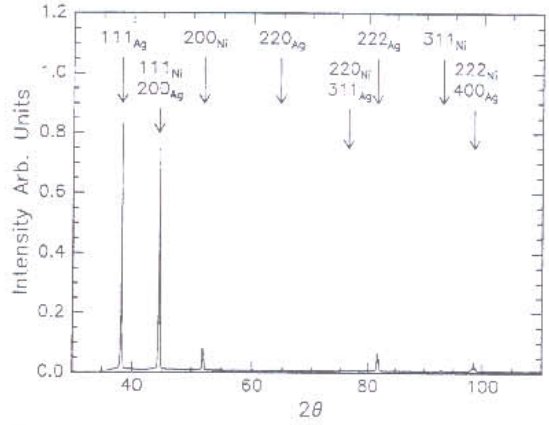

Fig. 2. X-ray scan (θ–2θ) of a creep-tested multilayer using Cu K_α radiation. The scattering vector is perpendicular to the layers. A strong (111) texture is evident for both Ag and Ni. For randomly oriented grains the $(200)_{Ag}$ peak would have 42%, and the $(311)_{Ag}$ and $(220)_{Ag}$ peaks would each have 20%, of the integrated intensity of the $(111)_{Ag}$ peak; the same applies to the nickel peaks.

X-ray diffraction pattern of Fig. 2 shows that both the silver and nickel layers have a strong (111) texture [11]. The cross-sectional electron micrograph of Fig. 3 shows adjacent silver and nickel grains with twin boundaries running continuously through both of them. This demonstrates the epitaxial relation between the grains. Therefore the interfaces under investigation are primarily of the (111) epitaxial type.

For testing, the films were mounted inside a steel furnace block, which opens up to allow the mounting of a film on the inner side of one of the halves. As seen in Fig. 4 the ends of the dogbone samples are clamped into the top and bottom invar grips. To insure good gripping, the clamp surfaces are coated with a fresh slurry of 1 μm alumina grit and distilled water before each run. The lower grip is permanently attached to one half of the furnace block. The grip itself sticks out of the furnace block and rests on insulators that in turn rest on the steel base plate of the vacuum

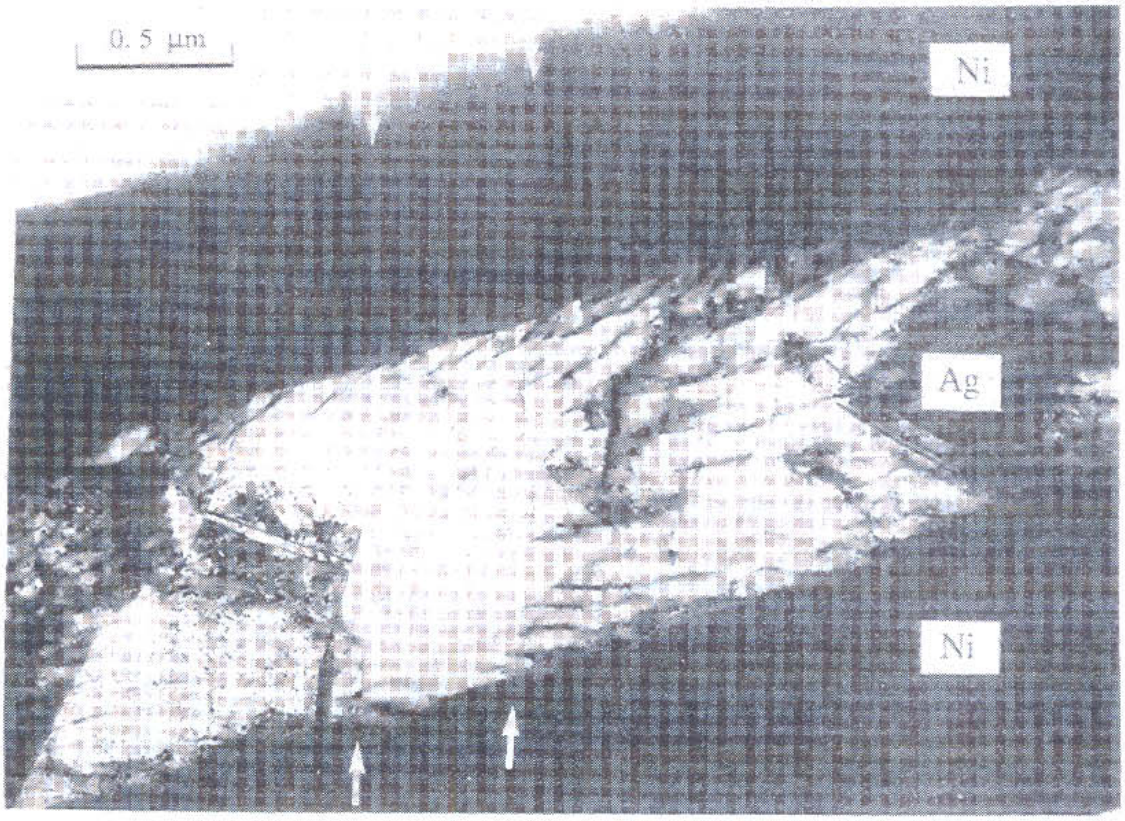

Fig. 3. Cross-section TEM image of a creep-tested film. Twin boundaries are marked between opposing arrows. Note that they run continuously through adjacent silver and nickel layers.

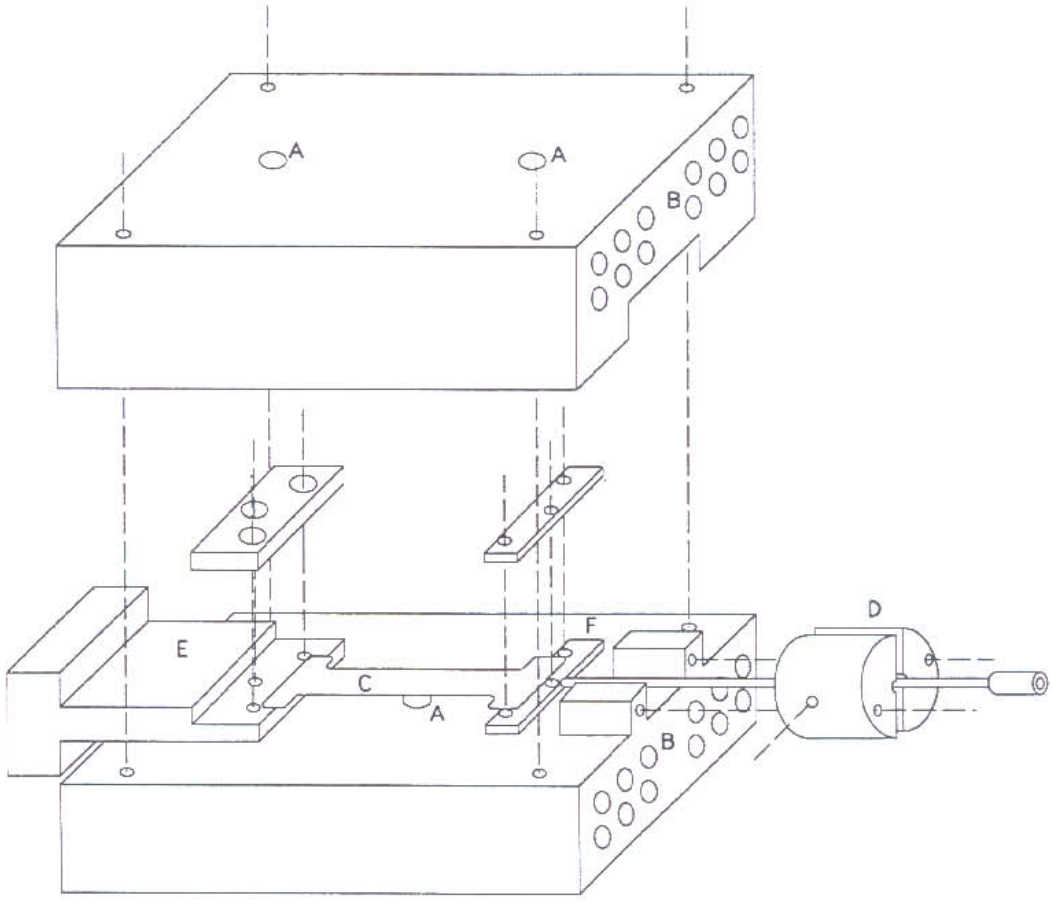

Fig. 4. The furnace assembly used for tensile creep testing of free-standing thin films. The two main blocks have holes for thermocouples (A) and heater wires (B). The film (C) is immobilized for transport using the half-annular pieces (D). The furnace stands on the lower grip (E). The upper grip (F) sticks out of the furnace and is attached to the balance beam in Fig. 5.

chamber. The upper grip is welded to an invar rod that sticks through a hole in the furnace block. The invar rod is threaded onto an aluminum rod that can be hung from one knife edge of a balance beam. From the knife edge on the other side of the balance beam hangs an aluminum rod, onto which a length of iron rod is screwed. The change in the length of the sample is detected by the displacement of this iron core inside a linear voltage-displacement transducer (LVDT). The base load for the run is attached beneath the iron rod, and an additional ("toggling") load is added or removed from the top of the balance beam above the LVDT (see Fig. 5). The support of the balance beam, which was kept at constant temperature with cooling coils, and the grips were also made of invar. The accuracy of the length measurements was limited by mechanical noise in the room and thermal fluctuations of the furnace, rather than by the resolution of the LVDT. The smallest displacement recorded was 0.125 μm, corresponding to a strain increment of 5×10^{-6}. The elongation and temperature were recorded automatically by a computer. The entire assembly was inside a bell jar that was diffusion pumped during runs. Aside from the first few hours after the initial heat up, during which pressures increased into the low 10^{-5} torr range and then steadily decreased, the pressure during all runs was less than 4×10^{-7} torr. The furnace was surrounded by sheets of copper shim as radiation baffles. Enough shim was used to minimize the heat loss and have a reasonably uniform temperature as registered by the thermocouples placed along the length of the film (see Fig. 4). Their readings were typically within 3°C. The temperature of the furnace was stable to within ± 2°C during the creep runs.

3. RESULTS

3.1. *Transient effects*

Most runs were started by heating a sample in the evacuated apparatus with a load less than the anticipated value of P_0, the zero creep load. Nonetheless, during the heat-up, and for some time afterwards, the film continued to lengthen, with a decreasing strain rate that eventually became negative. A substantial portion of this lengthening was due to thermal transients in the apparatus.

A second contribution to the initial transient is grain growth. The zero creep load P_0 of a film depends on the ratio of the grain width W and thickness T, which is equal to the layer thickness (columnar grains) [4]. P_0 increases monotonically with the ratio W/T to $2W_{film}\gamma_{Ag\text{-}Ni}$ per bilayer (W_{film} is the width of the film). Growth of the columnar grains in the lateral direction increases W/T, and hence also P_0. As P_0 increases toward the actual load P, the strain rate, which is proportional to $(P - P_0)$, decreases with time, and eventually becomes negative. This continues until grain growth in the two-dimensional layers stagnates [5].

An additional transient, in which the strain rate temporarily became more *negative* than the steady state value, was observed after the initial heat-up and grain growth transients had subsided. It is thought to be the result of the difference in the thermal expansion coefficient, which is larger for silver than for nickel. Heat-up therefore results in a compressive stress in the silver layers and a tensile stress in the nickel layers. Because the silver layers are under compression, and the silver flows more rapidly, the multilayer shrinks until the thermal mismatch has been accommodated. Thus, this transient manifests itself by a temporarily high negative contribution to the strain rate. An estimate of the total strain due to thermal mismatch is similar to the total negative strain contribution observed in the creep transient [6].

3.2. *Load changes*

Once a reliable steady state strain rate was established, the applied load was changed by adding the toggling load. An instantaneous displacement resulted due to the elastic response of the film and possible compliance of the apparatus. This was

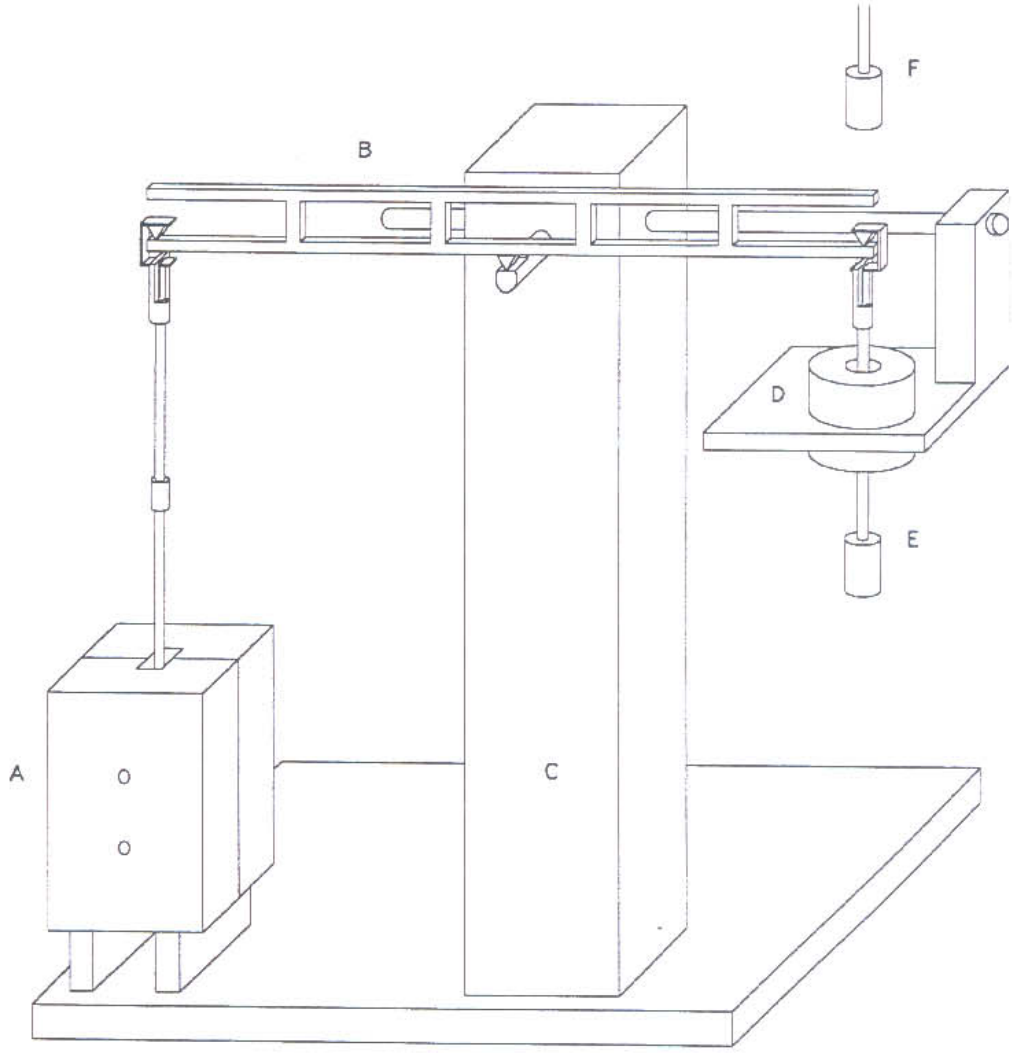

Fig. 5. The apparatus used for tensile creep testing of free-standing thin films. The furnace block (A) is that of Fig. 4; the balance beam (B) is supported by the invar rod (C). The LVDT (D) detects the motion of the iron core suspended inside it. The base load (E) hangs under the iron core. The toggling load (F) is shown suspended above the balance beam. The entire assembly is contained in a diffusion-pumped bell jar.

followed by a transient during which the strain rate decreased with time, resulting in a regime of constant strain rate. At this point the toggling load was removed and an identical response, with a negative sign on the strain rate, followed. This loading and unloading cycle was repeated as many times as possible. Figures 6(a) and (b) show typical creep data with multiple togglings of the load on a sample. These data show that for load changes of ± 20 g the total transient strain is about 10^{-3}. Since the relaxation of the elastic mismatch between the silver and the nickel produces no more than 10^{-5} strain [6], most of the transient is likely of anelastic origin.

In order to achieve better accuracy, most values of the zero creep load were determined by interpolation rather than extrapolation. Initial loads were below the anticipated value of P_0, and the toggling load was selected to make the total load greater than P_0. The base load and toggling load used depended on both the number of interfaces and the thickness of the layers in the sample. Because twelve nominally identical samples were made in each deposition run, several identical samples could be tested with different base loads, and usually different toggling loads, to check that the strain rate depended linearly on the load. The results of creep experiments on five identical films are shown in Fig. 7. The variation in P_0 is less than 10% even though the strain rates vary by a factor of 2.5. For the experiments in this work, base loads ranged from 2.0 to 20.0 g, and toggling loads ranged between 5.0 and 20.0 g.

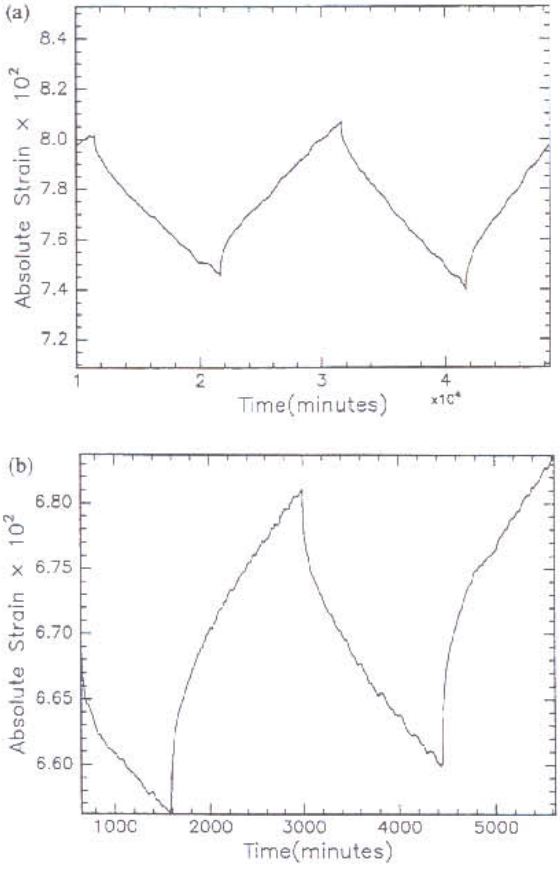

Fig. 6. Elongation–time data from the creep tests of two silver–nickel multilayers. (a) Run v5-23-91 at 650°C of a film with 15 bilayers. The loads were 10.0 g (negative strain rate) and 30.0 g (positive strain rate). (b) Run v9-6-91 at 699°C of a film with 8 bilayers. The loads were 2.0 (negative strain rate) and 22.0 g (positive strain rate). Note the marked anelastic transient.

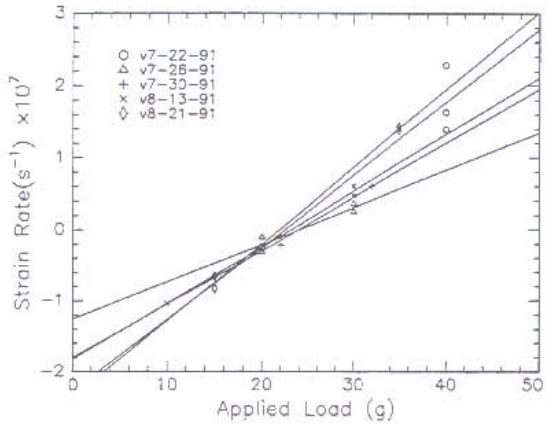

Fig. 7. Steady state strain rate vs load for runs on five 21 bilayer silver–nickel films, showing the determination of the zero creep load by interpolation between positive and negative strain rates. Though the slopes vary by a factor of 2.5, the zero creep loads vary by only 10%.

3.3. *Degradation of the layers*

It was observed that P_0 decreased toward the end of longer runs: for the same loads the positive strain rates increased, and the negative ones became less negative. Observation of the cross-section of each sample by scanning electron microscopy (SEM) after the creep test established that the decrease in P_0 corresponded to a breakdown of the layer structure (see Fig. 8) and is the result of a decrease in the vertical "active" interface area. In some runs the bilayer structure broke down completely, all the way to full "beading" of the nickel layers.

Limited beading is no problem. In fact, it occurs for the same reasons that it occurs in homogeneous wire samples [7]. It can, however, lead to two problems: (1) the beading nickel grain impinges on a

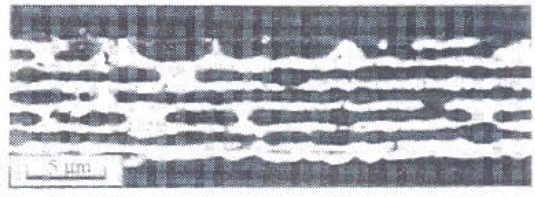

Fig. 8. SEM image of a portion of the cross-section of a creep tested film with a degraded layer structure: nickel grains (dark phase) in adjacent layers impinge, "pinch-off" occurs in the nickel layers (formation of a hole; see also Fig. 11), and most of the silver in the subsurface layers has been lost by evaporation. The data from such samples was not used.

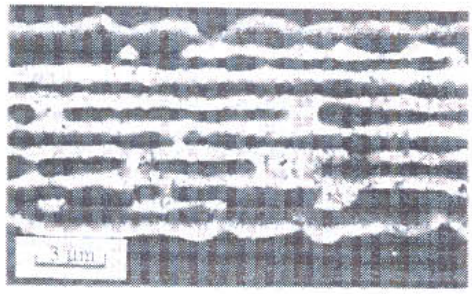

Fig. 9. SEM image of a portion of the cross-section of a creep tested film (run v11-7-90) consisting of 9 bilayers of silver–nickel tested between 673 and 697°C. Some beading and pinch off of the nickel layers is evident, and evaporation of the subsurface silver layers is severe. The layer structure is still well defined, however, and the creep data could be used.

nickel grain in an adjacent layer and creates a hole in the silver layer, or (2) the nickel grains pinch off at a grain boundary, leaving a hole in the nickel layer.

The evaporation of the outermost silver layers at elevated temperature has already been mentioned. The completely or partially depleted outer silver layers are obvious in the cross-section. Silver depletion was a problem only at 800°C and above. The appearance of silver deposits in the furnace indicated that this was due to the high vapor pressure of silver at these temperatures. This problem was remedied by making nickel the outer layer, by the incorporation of the sacrificial silver subsurface layer, by the intentional deposition of silver on the furnace to satisfy the equilibrium vapor requirements, and by performing most experiments at 700°C. For higher temperature runs, the time was kept short. This was accomplished by using loads that were farther from P_0, for larger strain rates, and by toggling loads after smaller net strains.

The first samples tested had bilayer thicknesses of 0.06–0.1 μm with hundreds of bilayers. Unfortunately, they only lifted a load for a limited time, i.e. P_0 decreased rapidly with time. Cross-sectional transmission electron microscopy (TEM) showed that nearly complete breakdown of the layered structure occurred at relatively small strains. For example, a film with 175 bilayers, each layer 0.04 μm thick, after shrinking just 0.7% with a 5.0 g load during 400 minutes at 450°C, began to exhibit a positive strain rate.

Most of the films tested had 1.0 μm thick bilayers. Figure 9 shows an example of a specimen that maintained a well-defined layer structure after 2 heating cycles, and 5 load changes between 2.0 and 12.0 g during 5500 min at 700°C with a cumulative strain of -3.0%.

In a film with 2.6 μm thick bilayers, no evidence of breakdown was seen after 7 load changes between 2.0 and 22.0 g, with strains of $\pm 0.3\%$ and larger, during 7000 min at 720°C and an additional 200 min at 800°C. Figure 13 is another example of a layer structure with limited beading (groove formation) that remained intact for an extended period of time and provided good data.

3.4. Steady state creep data

Since some of the films had silver outer surfaces and others nickel ones, a correction needed to be made for the free surface tensions. This was done on Fig. 10 by using the average values of the surface tensions for the pure elements [8]. Since the resulting plot is a straight line through the origin, the free surface tensions in these experiments must be close to the literature values.

Alternately, the uncorrected values of P_0 for films with nickel surfaces could have been plotted vs N. The intercept of the resulting straight line through the data would have given the effective free surface tension in these experiments—close to the literature value. The same could, in principle, have been done for the films with silver surfaces. Unfortunately, the zero creep experiments on films with silver surfaces suffered greatly from layer deterioration. For this reason few results from these runs are retained here. In addition, these samples had relatively few bilayers. Because of these problems, extrapolation to $N = 0$ was not reliable. The corrected plot (Fig. 10) was used here, since it allows both data sets to be combined. It should be kept in mind that only the *slope* of the $P_0(N)$ plot is important for the determination of the interfacial tension. For the data of Fig. 10 it is 0.93 ± 0.018 g/bilayer.

To test the free surface tension for silver under the present experimental conditions, the zero creep load of two 6 μm thick films was determined, and found, within the error, to be equal to the literature value (see Fig. 10).

Plots of the corrected zero creep load *per bilayer* vs the total film thickness or the number of bilayers

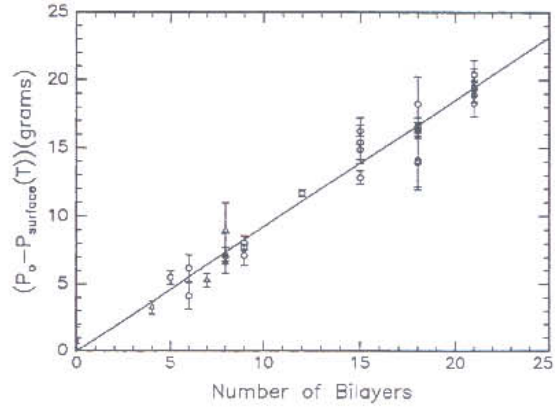

Fig. 10. The dependence of the zero creep load P_0, corrected for the contribution from the free surfaces, on the number of bilayers. Only the data for films with repeat lengths less than 1.5 μm (circles) are included in the linear fit, though all results are shown. This selection was made because the aspect ratio of the grains, W/T, was found to depend slightly on the repeat length. The fit gives a slope of 0.93 ± 0.018 g/bilayer.

Table 1. Creep test data

Sample	N	P_0 (g)	ΔP_0 (g)	P_s (g)	T_b (μm)	T_{film} (μm)	T_{Low} (°C)	T_{High} (°C)	W/T
v10-5-90	6	8.43	1.0	2.25	1.16	7.6	686	699	(2.7)
v10-30-90	0	2.65	0.5	2.25	—	6.4	588	609	(2.7)
v11-7-90	9	11.69	0.5	3.6	1.13	10.7	673	697	(2.7)
v11-14-90	9	10.76	0.75	3.6	1.08	10.3	683	697	(2.7)
v12-7-90	12	15.4	0.25	3.6	1.08	13.5	669	678	(2.7)
v12-14-90	5	7.8	0.5	2.25	1.16	6.4	676	686	(2.7)
v1-7-91	0	3.3	1.0	2.25	—	(6.0)	638	643	(2.7)
v1-25-91	4	7.0	0.5	3.6	(2.0)	(9.0)	652	678	2.2
v4-8-91	9	11.2	0.25	3.6	1.05	10.0	697	719	(2.7)
v4-15-91	7	8.8	0.5	3.6	(2.0)	(15.0)	707	713	(2.2)
v4-30-91	15	18.4	1.0	3.6	(1.2)	(19.8)	701	711	(2.7)
v5-7-91	15	19.8	1.0	3.6	(1.2)	(19.8)	695	706	2.7
v5-14-91	15	16.4	0.5	3.6	(1.2)	(19.8)	697	702	(2.7)
v5-18-91	6	7.7	1.0	3.6	(1.5)	(9.8)	700	703	(2.7)
v5-23-91	15	19.3	1.25	3.6	(1.2)	(19.8)	652	655	(2.7)
v7-8-91	18	21.8	2.0	3.6	1.44	28.1	701	707	2.7
v7-11-91	18	20.2	0.25	3.6	1.33	25.9	701	705	(2.7)
v7-22-91	21	22.5	0.5	3.6	1.06	23.8	682	696	(2.7)
v7-26-91	21	24.1	1.0	3.6	1.06	23.9	692	694	(2.7)
v7-30-91	21	24.0	0.5	3.6	1.02	22.9	691	695	(2.7)
v8-13-91	21	23.1	0.5	3.6	1.07	24.1	696	700	(2.7)
v8-21-91	21	21.9	1.0	3.6	0.95	21.3	699	701	(2.7)
v8-28-91	8	10.3	0.25	3.6	2.53	24.0	698	702	(2.2)
v9-6-91	8	10.8	0.5	3.6	2.82	26.8	697	701	2.2
v9-11-91	8	10.7	1.5	3.6	2.74	26.0	719	726	(2.2)
v9-30-91	18	17.7	2.0	3.6	1.27	24.8	698	702	2.7
v10-4-91.A	18	20.1	0.75	3.6	1.39	27.1	693	699	(2.7)
v10-4-91.B	18	16.9	2.0	3.6	1.39	27.1	787	795	(2.7)
v10-10-91	8	12.6	2.0	3.6	3.05	29.0	695	696	(2.2)
v12-9-91	21	22.9	0.5	3.6	1.17	26.3	690	704	(2.7)

Columns: (1) the sample number; (2) the number of bilayers, N; (3) the zero creep load, P_0; (4) the $\pm$ error, ΔP_0, of the zero creep load measurement; (5) the contribution P_s of the silver or nickel surfaces to the zero creep load from Jones [Ref. 8], (6) the bilayer thickness, T_b; (7) the thin film thickness, T_{film}; the bilayer and thin films thicknesses are determined by weight, except for bracketed ( ) thicknesses which are the nominal deposited thickness; (8) the lower bound on the test temperature T_{low}; (9) the upper bound on the test temperature, T_{high}; (10) the aspect ratios of the nickel grains, W/T, determined according to the procedure described in the test, except for bracketed ( ) values, which were taken equal to those in films with similar bilayer thickness T_b are used.

revealed no significant dependence. A small apparent increase in the corrected zero creep load per bilayer with bilayer thickness, 2% per μm, is most likely a manifestation of the improved layer integrity for thicker layers.

No statistically meaningful dependence of P_0 on temperature was found.

4. ANALYSIS AND DISCUSSION

4.1. Deformation mechanism

According on the deformation mechanism maps developed by Frost and Ashby [1], Coble creep is likely to dominate in these experiments. The observed strain rates, however, are approximately three orders of magnitude smaller than those predicted for the temperatures (700–800°C), grain sizes (0.5–1.0 μm), and stresses (0.5–2.0 MPa) used. This could be due to alloying or to interface-reaction-limited flow in the special (111) epitaxial interfaces in these samples [9].

Under the experimental conditions, the contribution to the strain rate in the nickel layers by bulk diffusion is smaller than that due to grain boundary diffusion by a factor of 10^5. Therefore, even with the apparent reduction by 10^3 in the contribution of grain boundary diffusion to the strain rate, Coble creep is still anticipated to be the dominant mechanism, and the analysis of the preceding paper should be used.

4.2. Flux model parameters

The interfacial tension, γ_{AgNi}, is obtained from the zero creep load per bilayer by the expression derived from the flux model in the preceding paper [4]

$$\gamma_{AgNi} = \frac{P_0}{2W_{film}\Phi^s} \tag{1}$$

where

$$\Phi^s(x, y) = \frac{x(2x - y)}{1 + x + 2x^2} \tag{2}$$

with $x = W_{Ni}/T_{Ni}$, the grain aspect ratio in the nickel layer, and $y = (\gamma_{Ag}x_{Ni}/x_{Ag} + \gamma_{Ni})/\gamma_{AgNi}$, the weighted ratio of the tensions. This formula is a limiting case of the more general expression that applies when one element is more mobile than the other. It can be used here because the mobility of the silver is much higher than that of the nickel.

Equation (2), for the zero creep load of a square-grain bilayer, is also the solution for a square-grain thin film, with a redefinition of the nondimensional interfacial tension variable y [4]. Based on this, the equation for the zero creep load of a hexagonal-grain thin film [4]:

$$\Phi^h(x, y) \equiv \frac{P_0}{2W_{film}\gamma_{AgNi}} = \frac{x(1.538x - 0.716y)}{1 + 1.074x - 1.538x^2} \tag{3}$$

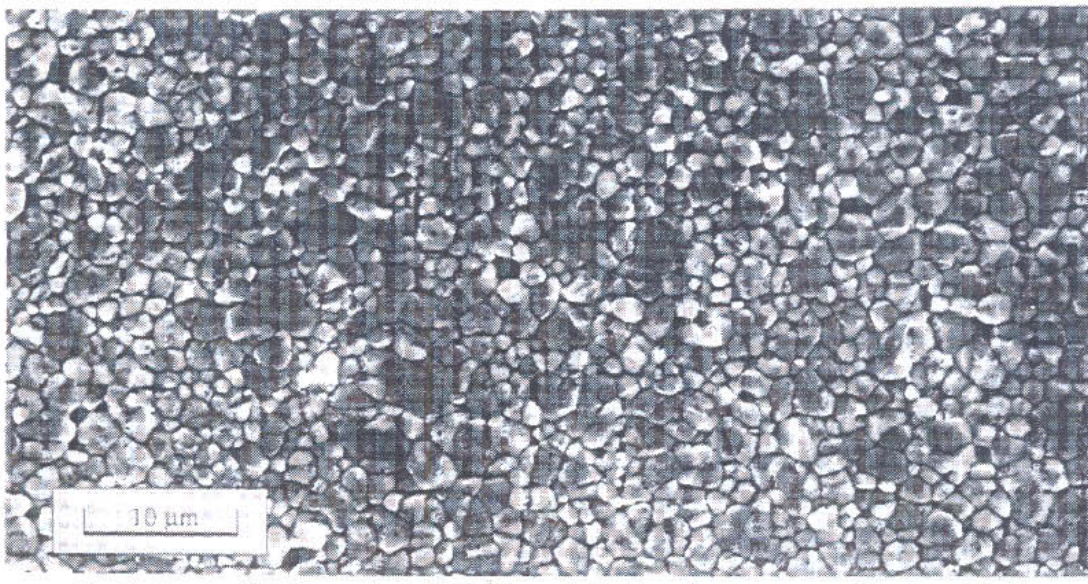

Fig. 11. Plan view SEM image of an individual internal nickel layer from a creep tested film (run v7-8-91). The grain boundaries are clearly marked by the grooves. The holes are the two-dimensional source of the pinch-off observed in the nickel layers in cross-section micrographs (Figs 8 and 9).

will be used for the hexagonal grain bilayer, with the same redefinition of y. The parameters x and y are obtained by measurements of the grain size and of grain boundary grooving, respectively.

4.2.1. Grain size. The average in-plane dimension W_{Ni} of the nickel grains was determined by scanning electron microscopy (SEM) on the internal nickel layers. To separate the nickel layers for plan-view examination, the silver was dissolved in hydrogen peroxide and ammonium hydroxide. All internal layers had nicely formed columnar grains that were easy to identify because of grain boundary grooving. Figure 11 shows an example. Inspection of some samples after short creep runs showed that the grains became columnar early in the runs. The average grain width, W_{Ni}, was determined from the average area, assuming square grains as in the flux model. Because the grains were columnar, the grain thickness, T_{Ni}, was set equal to the initial thickness of the deposited layer. Table 2 gives the values of T_{Ni} and W_{Ni}/T_{Ni}, and the number of grains counted for the determination, for the nickel layers in several films.

All layers in a film had similar numbers of grains per area (see Table 2 for two different layers in film v7-8-91). The aspect ratio between 2 and 3 is consistent with two-dimensional stagnated grain growth [10]. In some films, cross-bridging of the nickel layers prevented their separation even after the silver had been dissolved and made plan-view impossible. Therefore, because testing conditions (e.g. temperature and stress) were similar for all creep runs, the aspect ratios from Table 2 were assumed to be the same in all films tested. Thus $W_{Ni}/T_{Ni} = 2.7 \pm 0.2$ is used for all films with bilayer thickness $\leqslant 1.5\,\mu$m, while, for all films with bilayer thickness $\geqslant 2.0\,\mu$m, $W_{Ni}/T_{Ni} = 2.1 \pm 0.2$ is used.

Table 2. Measurements for the determination of the grain aspect ratio W_{Ni}/T_{Ni}

Sample	No. grains	Thickness (μm)	W/T
v5-7-91	654	(0.6)	2.7
v7-8-91 No. 1	1316	0.72	2.7
v7-8-91 No. 2	1297	0.72	2.6
v9-30-91	823	0.63	2.7
v1-25-91	237	(1.0)	2.2
v9-6-91	1229	1.41	2.1

Columns: (1) the sample number; (2) the number of grains counted for the determination; (3) the grain thickness as determined by the film weight, except bracketed thicknesses which are the nominal thickness deposited; (4) and the aspect ratio W/T.

Because no method was found to dissolve the nickel layers and leave the silver layers for examination, measurements of the aspect ratio W_{Ag}/T_{Ag} were restricted to cross-sectional TEM micrographs. Because all layers were equally thick, the aspect ratios of the nickel and silver grains were related by comparing the number of silver and nickel grains along sections of interface (see Fig. 12). Because there was no significant difference, the aspect ratio of the silver grains was set equal to that of the nickel grains in each film.

4.2.2. Grain boundary grooving. When a grain boundary in a layer meets the interface, a triple point develops. If the angle between the two parts of the interface is 2θ, the ratio of the tensions is

$$y = \frac{\gamma_{gb}}{\gamma_{AgNi}} = 2\cos\theta. \tag{4}$$

The average groove angle formed where nickel grain boundaries meet the silver–nickel interface was determined from three different types of SEM micrographs: (1) plan view of holes in the nickel layer, (2) polished cross sections, and (3) polished cross sections from which the silver layers had been dissolved

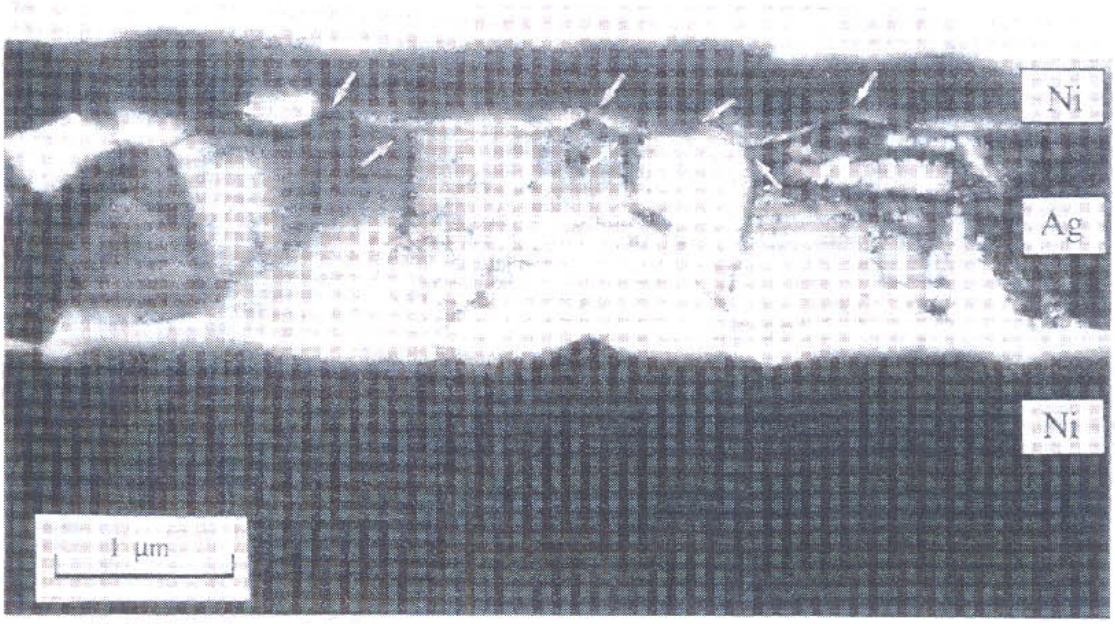

Fig. 12. TEM image of the cross-section of a creep tested film. The nickel and silver layers have been thinned to different thicknesses. Triple points at the nickel and silver grain boundaries are marked by the arrows near the interface.

and on which a thin (100 Å) layer of gold had then been sputter deposited to enhance the visibility of the remaining nickel layers (see Fig. 13). The results of the three types of measurements are summarized in Table 3.

Of the three techniques, the use of cross sections in which the silver layers have been dissolved allows the best determination of the orientation of the nickel grain boundary, in particular, whether or not it is perpendicular to the plane of the photo. If the grain boundary groove has no shadow behind it, it lies along the line of sight. In the micrographs of the plan-view holes, because the silver–nickel interface is three-dimensional, the grain boundary is more likely

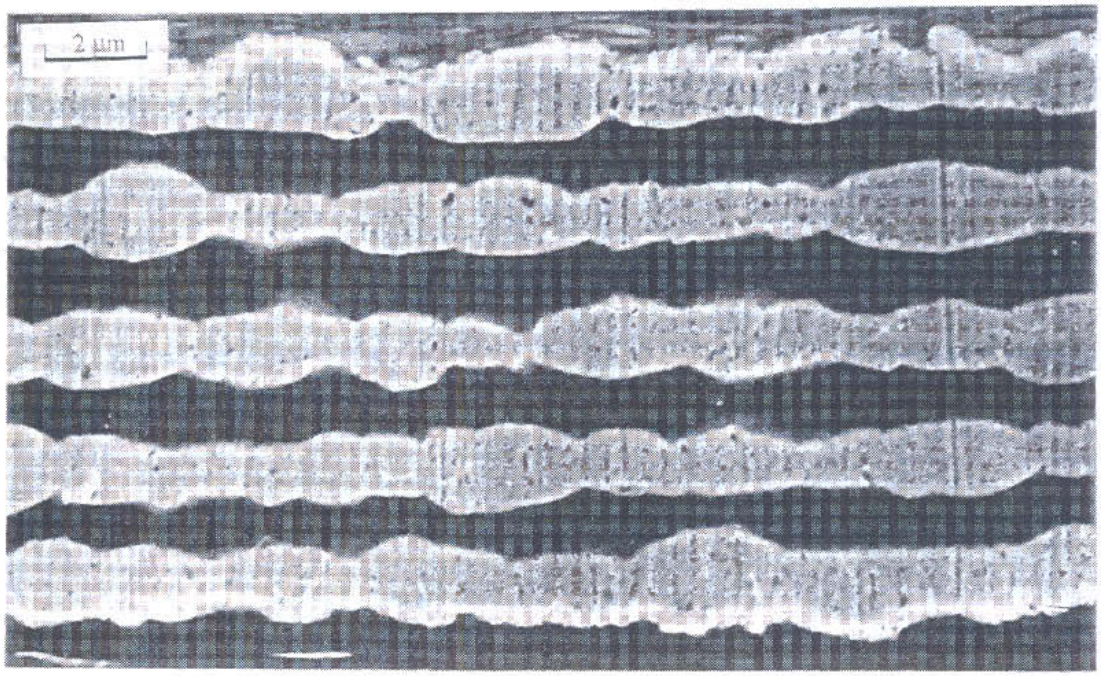

Fig. 13. SEM image of a portion of the cross-section of a creep tested film (run v1-25-91). The silver layers have been dissolved. The grooves at the grain boundaries in the nickel layers are clearly visible.

Table 3. Measurements for the determination of the tension ratio $\gamma_{NiNi}/\gamma_{AgNi}$

Technique	No. grooves	$2\bar{\theta}$ (deg)	σ (deg)	$\gamma_{NiNi}/\gamma_{AgNi}$
(1) Holes in plan view	12	120	11.3	1.00
(2) Unetched cross sections	30	122	8.9	0.97
(3) Etched cross sections	23	111	8.8	1.13

Columns: (1) The number of groove angles measured for the determination, (2) the average angle, (3) the standard deviation of the measurements, (4) the values for $\gamma_{NiNi}/\gamma_{AgNi}$.

to be perpendicular to the plane of the photo if its visible intersection with the silver–nickel interface is a straight line going away from the grain boundary groove. Averaging the data of Table 2 gives $118° \pm 10°$ for the groove angle, and, by equation (4), $\gamma_{NiNi}/\gamma_{AgNi} = 1.03 \pm 0.15$.

The triple points at silver grain boundaries could only be observed in cross-section TEM micrographs. The grooves at the silver boundaries were more shallow than those than the nickel grain boundaries (see Fig. 12). The average groove angle, 2θ, was found to be 168°, with a standard deviation of 11° from 36 observations, which may include a larger fraction of twin boundaries than in the nickel measurements. By equation (4), $\gamma_{AgAg}/\gamma_{AgNi} = 0.21 \pm 0.19$.

4.3. Evaluation of the interfacial tension and error analysis

The errors or uncertainties that arise in the determination of the interfacial tension γ_{AgNi} are associated with either the experiment or the theory. In the first category are: the error σ_P on the measured zero creep load, P_0, per length of silver–nickel interface; the errors $\sigma_R(Ag)$ and $\sigma_R(Ni)$ on the grain aspect ratios; and the errors $\sigma_\theta(Ag)$ and $\sigma_\theta(Ni)$ of the groove angle measurements. The second is the uncertainty σ_F arising from the assumptions made in the flux model. The total error, σ, on γ_{AgNi}, is taken, conservatively, as the sum of the individual errors.

4.3.1. Uncertainty from the assumptions in the model. Using equation (2) for the zero creep load per bilayer of a square grain bilayer film, with $P_0 = 0.93$ g/bilayer for films with $W_{Ni}/T_{Ni} = 2.7$ (Fig. 10), $W_{Ag}/T_{Ag} = 2.7$, $\gamma_{AgAg}/\gamma_{AgNi} = 0.21$, $\gamma_{NiNi}/\gamma_{AgNi} = 1.03$, and $W_{film} = 1.0$ cm, γ_{AgNi} is found to be 0.741 J/m^2. Substitution of the same parameters into equation (3) for the hexagonal grain bilayer film yields $\gamma_{AgNi} = 0.781$ J/m^2. Since the square and hexagonal grains approximate the observed equiaxed microstructure equally well, the average value $\gamma_{AgNi} = 0.76$ J/m^2 is used for the interfacial free energy. Half of the difference between the two values gives the uncertainty associated with the flux model itself, or $\sigma_F = 0.02$ J/m^2.

4.3.2. Error in the measurement of the zero creep load. Because the strain rate varied linearly with stress, the zero creep load P_0 was determined by linear interpolation using the relation

$$P_0 = P_B - P_T \frac{\dot{\epsilon}^-}{\dot{\epsilon}^+ - \dot{\epsilon}^-} \tag{5}$$

where $\dot{\epsilon}^-$ is the average strain rate observed with the base load P_B, and $\dot{\epsilon}^+$ is the average strain rate observed with the base load and toggling load P_T together. The uncertainty ΔP_0 is then

$$\Delta P_0 = P_T \frac{\Delta\dot{\epsilon}^- \dot{\epsilon}^+ - \Delta\dot{\epsilon}^+ \dot{\epsilon}^-}{(\dot{\epsilon}^+ - \dot{\epsilon}^-)^2}. \tag{6}$$

The uncertainties $\Delta\dot{\epsilon}^+$ and $\Delta\dot{\epsilon}^-$ were chosen to be half the difference between the largest and the smallest values for $\dot{\epsilon}^+$ and $\dot{\epsilon}^-$ respectively. Column ΔP_0 in Table 1 gives the uncertainty for each determination of P_0. In the fit of the dependence of the zero creep load on the number of bilayers in Fig. 10, the uncertainty in each zero creep load was represented by a standard deviation σ_i equal to ΔP_0. The resulting slope is $P_0 = 0.93 \pm 0.018$ g/bilayer. The corresponding error on γ_{AgNi} for both grain geometries is $\sigma_P = 0.014$ J/m^2 [equations (2) and (3)].

4.3.3. Error in the measurement of the aspect ratio of the grains. The error on the aspect ratio W_{Ni}/T_{Ni} was ± 0.2. The associated error in γ_{AgNi} is $\sigma_R(Ni) = 0.03$ J/m^2. The error on the aspect ratio W_{Ag}/T_{Ag} was ± 0.2. The associated error in γ_{AgNi} is $\sigma_R(Ag) = 0.003$ J/m^2.

4.3.4. Error in the measurement of the grain boundary groove angles. Using all the points in Table 3, the groove angle for the nickel grains is $118° \pm 10°$. This corresponds to an uncertainty in $\gamma_{NiNi}/\gamma_{AgNi}$ of ± 0.15 [see equation (4)]. The associated error in γ_{AgNi} is $\sigma_\theta(Ni) = 0.026$ J/m^2. The groove angle for the silver grains is $168° \pm 11°$. This corresponds to an uncertainty in $\gamma_{NiNi}/\gamma_{AgNi}$ of ± 0.19 [see equation (4)]. The associated error in γ_{AgNi} is $\sigma_\theta(Ag) = 0.031$ J/m^2.

4.3.5. Overall error. Summing σ_P, σ_F, $\sigma_R(Ni)$, $\sigma_R(Ag)$, $\sigma_\theta(Ni)$, and $\sigma_\theta(Ag)$ gives $\sigma = 0.12$ J/m^2 for the overall error in the determination of γ_{AgNi}. Thus the final result, $\gamma_{AgNi} = 0.76 \pm 0.12$ J/m^2, is obtained. This value is slightly higher than that in our earlier reports [6, 11] because additional corrections, in particular the effect of the grooving at the silver grain boundaries, have been applied.

5. CONCLUSION

This work demonstrates that it is possible to determine the interfacial tension directly by zero creep measurements on multilayers. The value found for the (111) epitaxial interface between silver and nickel, $\gamma_{AgNi}(111) = 0.76 \pm 0.12$ J/m^2, falls between the theoretical values of $\gamma_{AgNi}(111) = 0.42$ J/m^2 obtained by Gumbsch and Daw [2] and $\gamma_{AgNi}(111) = 0.96$ J/m^2 obtained by Streitz [3], though closer to the latter. An earlier experimental determination [12] of the *average* silver–nickel interfacial tension, based on groove

angle measurements, coarsening kinetics and the literature value of the average grain boundary energy in nickel, gave $\gamma_{Ag/N_i} = 0.80\ J/m^2$.

Acknowledgements—The authors gratefully acknowledge the experimental help provided by J. L. Bell, J. A. Ruud, A. V. Wagner and D. T. Wu. This work has been supported by the Office of Naval Research under contract number N00014-91-J-1281. D. Josell gratefully acknowledges the generous support of the Fannie and John Hertz Foundation.

REFERENCES

1. H. J. Frost and M. F. Ashby, *Deformation-Mechanism Maps: The Plasticity and Creep of Metals and Ceramics*. Pergamon Press, Oxford (1982).
2. P. Gumbsch and M. S. Daw, *Phys. Rev. B* **44**, 3934 (1991).
3. F. H. Streitz, personal communication from work related to his Ph.D. thesis, Johns Hopkins University (1992).
4. D. Josell and F. Spaepen, *Acta metall. mater.* **41**, 3007 (1993).
5. W. W. Mullins, *Acta metall.* **6**, 419 (1958).
6. D. Josell, Ph.D. thesis, Harvard Univ. (1992).
7. F. H. Buttner, H. Udin and J. Wulff, *Trans. A.I.M.E., J. Metals*, p. 1209, Dec. (1951).
8. H. Jones, *Metal Sci. J.* **5**, 15 (1971).
9. E. Arzt, M. F. Ashby and R. A. Verrall, *Acta metall.* **31**, 1977 (1983).
10. H. J. Frost, C. V. Thompson and D. T. Walton, *Acta metall.* **38**, 1455 (1990).
11. D. Josell and F. Spaepen, *Mater. Res. Soc. Symp. Proc.* **239**, 515 (1992).
12. S. C. Yang, G. T. Higgins and P. Nash, *Mater. Sci. Technol.* **8**, 10 (1992).